Applied Ocean Research 108 (2021) 102477

Contents lists available at ScienceDirect

Applied Ocean Research

journal homepage: www.elsevier.com/locate/apor

Investigation of moonpools as pitch motion reducing device

Lars Mikkel Utnes Reiersen [a], Trygve Kristiansen [*,a], Babak Ommani [b,c], Arnt Fredriksen [d]

[a] Dept. of Marine Technology, Norwegian University of Science and Technology (NTNU), Trondheim, Norway
[b] SINTEF Ocean, Norway
[c] NTNU AMOS, Trondheim, Norway
[d] Entail, Norway

ARTICLE INFO

Keywords:
Moonpool
Piston-mode resonance
Gap resonance
Freely floating body
Forced motion
Pitch motion cancellation
2D experiment

ABSTRACT

Moonpools as a device for reducing pitch motion is investigated experimentally, numerically and by an approximate theory. A two-dimensional study is carried out of a rectangular body with two moonpools. Forced heave and pitch motion, as well as freely floating body in regular waves are studied. The body geometry is varied; two drafts and five different moonpool inlet configurations are considered; rounded and squared inlets, as well as vertical plates (appendages) extending below the inlet with three different depths. The outer corners of the body are square. There is a resonance as well as cancellation period in both pitch and heave, where the cancellation is the desired effect. By cancellation period we refer to a narrow period range where the pitch motion is nearly cancelled, due to the pressures induced by the moonpool piston-mode resonance. Our investigation reveals that the cases with rounded and square moonpool inlet geometries are most efficient in cancelling the pitch motions.

1. Introduction

Moonpools may be exploited in order to reduce rigid body motions in a frequency range near the natural frequency of the moonpool piston mode. In (Fredriksen et al., 2016) the authors investigated a barge with two moonpools for reducing the pitch motions of floating bridge foundations at one of the main natural modes of the bridge. The present study is inspired by the need for better understanding the coupled system, and in particular the role of flow separation at the moonpool inlets. We present a study performed in a two-dimensional setting, including experiments, numerical simulations and theoretical work. A rectangular barge with two moonpools is investigated both in freely floating regular wave conditions, and forced heave and forced pitch motions. The results are compared to that of a similar barge without moonpool. Our main focus is the configuration of the moonpool inlet (i.e. the entrance of the moonpool at the bottom of the barge). It is well established that flow separation from the moonpool inlet represents a major part of piston-mode damping at piston-mode resonance. We therefore investigate rounded and square inlets, in addition to inlets with vertical plates extending vertically below the bottom of the body. In the case with rounded moonpool inlets, there is weak flow separation with resulting weak damping, and therefore efficient pitch cancellation only for a narrow frequency range. It was anticipated by the authors that the increased damping for the other configurations could increase the frequency range for which there is significant pitch motion reduction. However, our results show that the case with rounded moonpool inlet out-performs the configurations with vertical plates, and gives similar results as the case with square moonpool inlet.

It is well known that tanks partly filled with fluids may have a significant effect on the vessel motions, cf. for instance (Rognebakke and Faltinsen, 2003). The lowest sloshing frequency is the most important, since it is typically closest to frequencies with energy in the incident wave spectrum, it induces the highest loads on the vessel, and it excites higher modes due to nonlinear free-surface effects. Nonlinear sloshing easily occurs, with violent free-surface behaviour as (unwanted) consequence, in particular if the tank is long compared to the vessel. Nonlinear free-surface effects leading to super-harmonic excitation of sloshing is also documented for large moonpools (Ravinthrakumar et al., 2020). In this study the moonpool length was half the ship length. In addition to significant nonlinear sloshing in the moonpool, the first sloshing mode influenced strongly the surge, heave and pitch motions. It is known that moonpools with significant size affects the vessel motions. See for instance (Maisondieu and Boulluec, 2001) where they investigated a well-head barge with a relatively large moonpool. The moonpool significantly affected heave and pitch motions, and also surge and sway to some degree. In Fredriksen et al. (2015), a similar two-dimensional study as that in the present paper was performed with a body with one moonpool only, in the middle of the body. Cancellation and

* Corresponding author.

https://doi.org/10.1016/j.apor.2020.102477
Received 22 June 2020; Received in revised form 23 October 2020; Accepted 26 November 2020
Available online 13 January 2021

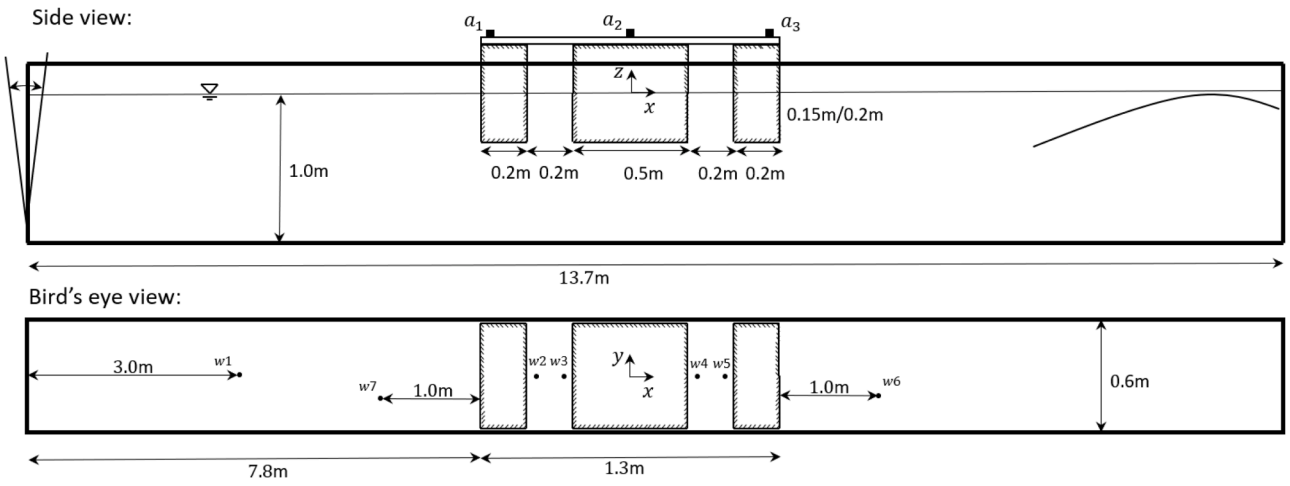

Fig. 1. Experimental set-up of the forced motion model tests and freely floating rigid motion model tests in regular waves. Top: side view. Bottom: bird's eye view. The total tank length is 13.7 m, and the tank width 0.6 m. The model is $B = 1.3$ m long and 0.592 m wide. The moonpool gap widths are $b = 0.2$ m. Two drafts of $D = 0.15$ m and 0.2 m were tested in the force motion test. In the freely floating tests, only $D = 0.15$ m was tested. The locations of the wave probes (w1 - w7) are provided. Wave probe w1 is used to measure the incident wave. Three accelerometers were mounted on the top of the model; a_1 and a_3 are vertical and a_2 horizontal. The mooring lines were not included in the forced motion tests. In the forced motion tests, a parabolic beach was installed also on the left hand side of the flume.

resonance periods for heave only, and not pitch, was observed for that configuration. The use of moonpools as motion reduction device is also exploited in floating offshore wind turbine design, such as that by Ideol.

A benefit of using several small moonpools rather than closed tanks as damping device, is that there is significantly less potential for violent sloshing. Energy can escape due to radiated waves, and dissipate through flow separation at the moonpool inlet. In order to have a significant effect on pitch motions, the moonpool must in practice affect the pressure underneath the ends of the body. This may be achieved by a large moonpool. A large moonpool, however, may exhibit the first sloshing period within the wave spectrum. Further, a large moonpool reduces the dead-weight. Two or more laterally placed moonpools achieves both large effects in pitch, as well as keeping only the (non-violent) piston-mode motion within the incident wave spectrum range. This is exploited in the present concept. The pitch cancellation period can be tuned by varying the draft of the body, moonpool width and moonpool position. A resonance period in the vicinity of the cancellation period is an (unwanted) side-effect of the moonpools.

Dedicated experiments are carried out, with corresponding numerical simulations for selected cases. The study involves forced pitch and heave motions, as well as freely floating, horizontally moored, body in waves.Simulations of the forced motion cases are carried out by the Potential Viscous Code (*PVC*) (Kristiansen and Faltinsen, 2015), while for the freely floating body cases, simulations are carried out using the code by Fredriksen et al. (2015), which is based on a similar numerical hybrid scheme. In these methods, the free-surface conditions are derived from a potential flow theory assumption, but we emphasize that both codes are based on a Navier Stokes solver in the domain covering the body, such that the flow is (in principle) solved for by first principles, and there is no artifical or empirical damping added. Also, an approximate theory, similar to that by Molin (2001) is developed to explain the two different piston-mode natural frequencies in forced heave and pitch.

The present paper is organised as follows. The experiments are described in Section 2. Next, the numerical methods are briefly described in Section 3. The approximate theory is presented in Section 4. The experimental and numerical results are presented in Section 5. Last, concluding remarks are given in Section 6.

2. Experiments

The model tests were performed in a glass-walled wave flume located at the Marine Technology Centre at NTNU in Trondheim. The model setup is illustrated schematically in Fig. 1. Model scale dimensions are presented in Table 1. Two photos are provided in Fig. 2. Both forced motion and freely floating tests in waves were performed. A vertical actuator with a motion controller was used to oscillate the model. In the forced pitch motion tests, the pitch axis was taken in the still water line, and the middle of the model.

Table 1
Parameters describing the forced heave and forced pitch motion test set-up. The quantities are explained in Fig. 1.

Quantity	Parameter	Value
Beam of the model [m]	B	1.300
Beam of center box [m]	L_2	0.500
Beam of lateral boxes [m]	L_1	0.200
Total height of boxes [m]	H_m	0.400
Transverse width of boxes [m]	l_w	0.592
Moonpool gap width [m]	b	0.200
Draft [m]	D	0.150, 0.200
Water depth [m]	h	1.00

Five different moonpool inlet geometries were tested, see Fig. 3. In Fig. 3 we illustrate the terminology that we use throughout the paper; (a) moonpool inlet (area), (b) moonpool inlet geometry and (c) flow separation from the moonpool inlets. In the rounded moonpool inlet case, there is no or very weak flow separation given the significant radius of the inlet, r_m, relative to the piston-mode flow amplitude. Therefore, no no flow separation is indicated there.

An imagined model scale was chosen to be 1:256, corresponding to a full scale beam of 333 m and drafts of 51 m and 38 m. Due to the fact that the geometries involve sharp corners (except for the rounded moonpool inlet), scale effects are argued to be small since the separation points are fixed. Flow separation at the moonpool inlet is well known to contribute significantly to piston-mode damping. Further, flow separation from the two lateral bilge corners (marked by *A* in Fig. 2) of the model is expected to contribute to pitch damping.

2.1. Instrumentation

All data from the experiments were sampled at 200Hz. An amplifier of type Hottinger MGC+ was used for the data acquisition. A Butterworth filter with cut-off frequency at 20Hz was applied to all signals,

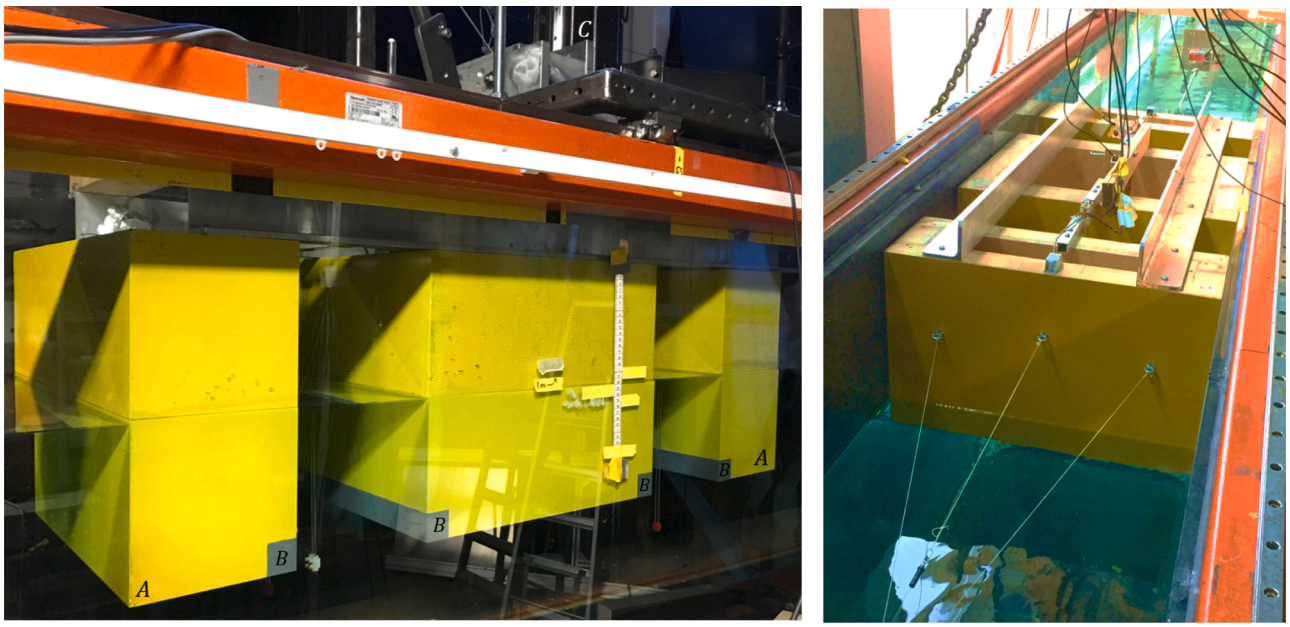

Fig. 2. Photos from the experimental set-up. Left: forced motion test with square moonpool inlets. Right: freely floating model test. *A*: the lateral bilges of the model. *B*: the 4 cm × 4 cm removable moonpool inlet pieces. *C*: the lower part of the actuator (in the upper part of the photo).

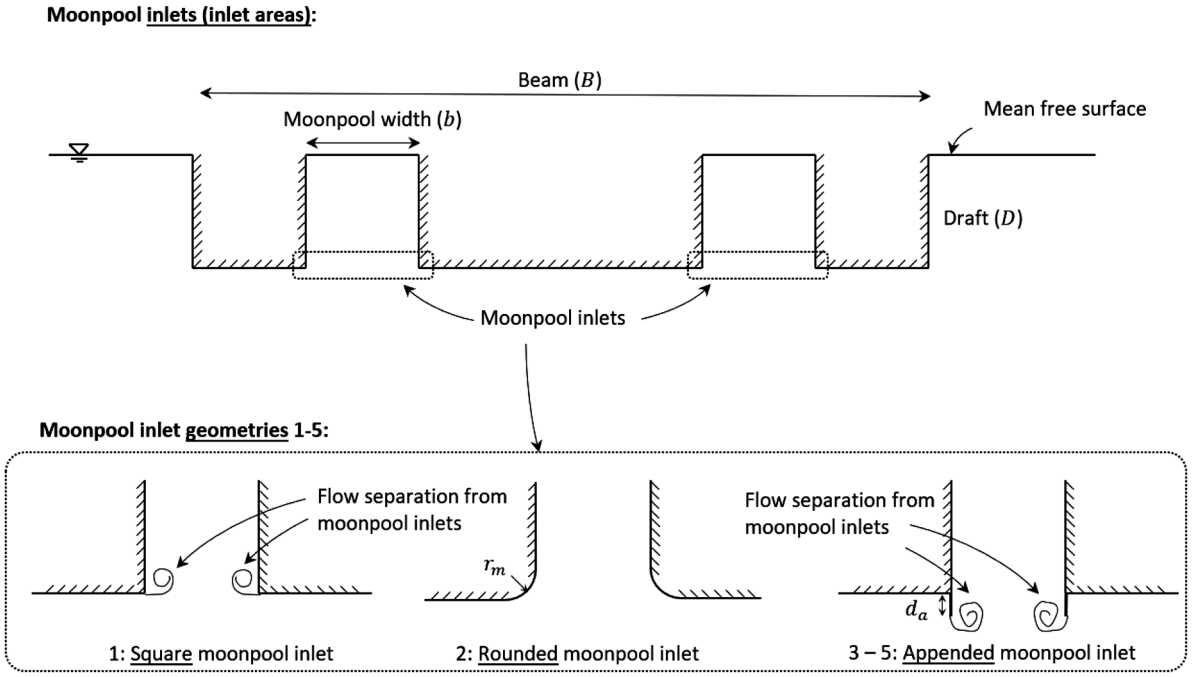

Fig. 3. Upper: Side view sketch of the model, which is a rectangular barge with two moonpools. The two areas that we refer to as 'moonpool inlet' are indicated by the dashed rectangles. Lower: mooonpool inlets. Five different moonpool inlet *geometries* were tested; squared, rounded and three different appendages. The radius of the rounded inlet was $r_m/b = 1/5$ ($r_m = 0.04$ m model scale). The appendages were vertical plates extending a distance d_a from the lower part of the boxes; $d_a/b = 0.05,\ 0.1,\ 0.15$ for the three cases denoted App1, App2 and App3, respectively (corresponding to 0.01 m, 0.02 m and 0.03 m in model scale). Flow separation from the moonpool inlets, which is a main contributor to piston-mode damping, is illustrated by rolled-up vortex sheets.

standard to most tests of this type. The accelerometers were designed by SINTEF Ocean with a maximum acceleration of $5g$, where g is the acceleration of gravity. They are known to be stable and accurate for the present wave/oscillation frequencies and (small) motion amplitudes. The wave maker and actuators were controlled by a-priori generated time-signals with up-date frequency of 50Hz. The wave gauges were standard capacitance wave staffs, i.e. two parallel steel bars of 2 mm diameter each, approximately 20 mm apart.

2.2. Forced heave and pitch experiments

The motivation behind the forced motion tests was to investigate the resonant response in the moonpools, with emphasis on the damping due to flow separation, without the complication of incident waves and body motions. The model was forced to move in heave and pitch separately. The vertical position of the fixed point of rotation was chosen at the still water line. In addition to two drafts, five different inlet configurations

Table 2
Parameters describing the freely floating test set-up. r_{yy} was estimated during the experiments by summing weight contributions.

Quantity	Parameter	Value
Draft [m]	D	0.15
Total model mass [kg]	m	79.92
Radius of gyration [-]	r_{yy}/B	[0.24, 0.36]
Pitch moment of inertia [kg m^2]	I_{55}	[7.75, 17.66]
Center of gravity (from model bottom) [m]	z_{CoG}	0.17
Spring constant [N/m]	s_1	27.4
Spring constant [N/m]	s_2	32.14
Pre-tension [N]	F_1	6.75
Pre-tension [N]	F_2	6.91
Mooring length [m]		1.52
Distance mooring line to still water line [m]		0.1

were tested at three forced motion amplitudes. The inlet configurations were changed by replacing a 40 mm × 40 mm removable section at the four moonpool inlet corners with the components illustrated in Fig. 3.

Four parameters were varied during the experiments; the draft (D = 0.2 m and D = 0.15 m), the oscillation period (30 different periods between 0.7 s and 1.54 s), the forced oscillation amplitude, and moonpool inlet geometry. The forced heave motion amplitudes were η_{3a} = 0.0025 m, 0.005 m and 0.0075 m, corresponding to non-dimensional heave amplitudes of $\eta_{3a}/B = 0.0019,\ 0.0038$ and 0.0058. The forced pitch motion angle amplitudes were $\eta_{5a} = 0.76,\ 1.01$ and 1.53 degrees, corresponding to non-dimensional vertical motion in the center of the moonpools of $b'\eta_{5a}/B = 0.0020,\ 0.0027$ and 0.0038 (somewhat lower than for forced heave). b' is the horizontal distance from the pivot point at the center of the model to the middle of the moonpools.

In total, almost 1 800 forced motion tests, including repetition tests, were performed. An automated controller set-up was designed in order to facilitate the test program. Only selected results are presented, chosen such as to reflect the main findings of the study. Five forcing periods was used to reach desired forced motion amplitude, followed by 50 consecutive steady-state motion oscillations until the motion decreased linearly to zero during five oscillations. The model was then held at rest for 200 s prior to the next test, which was found sufficient to reach calm conditions prior to the next run.

Seven wave probes were installed. Their locations are given in Fig. 1. Wave probes 1, 6 and 7 were mounted to the tank wall, whereas wave probes 2–5 were mounted to the moonpool hull, 6 cm from the hull. The free-surface was converted to Earth-fixed coordinate system using the recorded rigid-body motions. An Earth-fixed displacement sensor was mounted to the carriage to measure the forced motions.

For the forced oscillation experiments, the wave flume was equipped with a parabolic beach at each end. The upper position of these were approximately 1 mm below the free surface. This has been found to absorb the small-amplitude waves adequately (Kristiansen and Faltinsen, 2012). In the tests with waves, the beach in front of the wave maker was removed.

2.3. Freely floating experiments

About 900 regular wave tests were conducted, including repetition tests. This included 30 different wave periods (T = 0.7 s - 1.3 s), three different wave steepnesses ($H/\lambda = 1/60,\ 1/45$ and $1/30$) and two different radii of gyration of $r_{yy}/B = 0.24$ and $r_{yy}/B = 0.36$. Here, H is the wave height and λ is the wave length according to linear wave theory. Also for these tests, all the five inlet configurations were tested. Only one draft was tested in the freely floating tests; the lowest draft of $B/D = 8.7$. Two aluminum L-profiles were used to connect the three hulls. In total, 34.0 kg of lead weights was placed inside the boxes, making the total weight 79.9 kg (giving a draft of 15 cm). See Table 2 for descriptive parameters of the model and test set-up

Horizontal springs from both sides of the hull were connected to racks mounted to the tank wall 1.52 m away from the lateral walls of the hull. The model was thus free to move in surge, heave and pitch. Force rings were mounted on the mooring lines in-between the springs and the model. The springs were pre-tensioned such that no slack occurred during the tests. A soft mooring was used. The natural period in surge was 5.5 s, which is well outside the tested wave range. The pre-tension was 2.1N, and the vertical position of the mooring attachment was close to the centre of gravity of the model. The springs were modelled in the numerical simulations.

The model front was 7.8 m from the wavemaker. The wavemaker was programmed to generate 27 waves, then held at rest for 210 s before the next test. The number of wave periods was in general sufficient to obtain near steady-state rigid-body motions.

In the wave tests, an additional wave probe (wave probe 1), was positioned 3 m from the wavemaker. Wave calibration tests were carried out without the model, prior to the tests with model. The repeatability of the waves measured at this wave gauge relative to that wave calibration tests was found to be good.

Three accelerometers were mounted on the top part of the model in order to measure the rigid body motions; vertical accelerometer 1 and 3, and horizontal accelerometer 2 (cf. Fig. 1). The center-to-center distance between accelerometers 1 and 3 was 1.20 m. All motions were thus measured in a body-fixed coordinate system and later transformed to an Earth-fixed system. Importantly, one must remove the $g-$ component from the horizontal (body-fixed) accelerometer signal.

2.3.1. Brief discussion on error sources

Wave re-reflections by the wavemaker was a concern due to the relatively short distance between the front of the model and the wave-

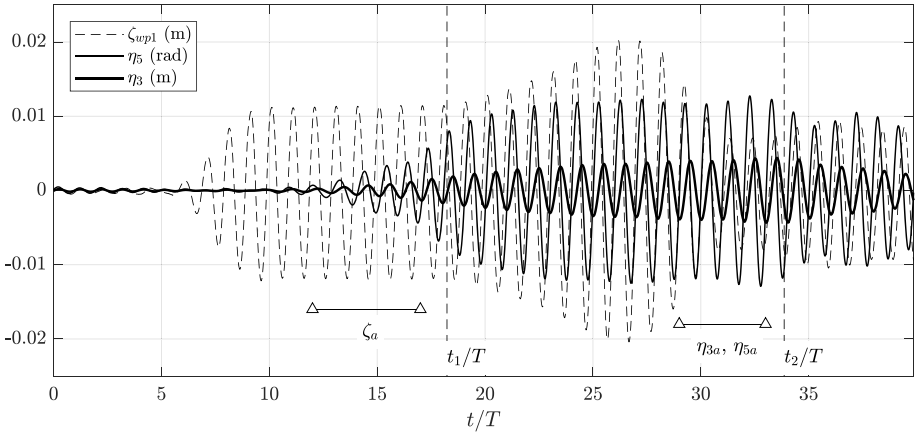

Fig. 4. Time-series of wave probe 1 (3 m from the wave-maker), heave and pitch motions in freely floating tests with wave steepness $H/\lambda = 1/60$, wave period T = 0.94 s (T^* = 6.58), draft B/D = 8.7 m and lowest radius of gyration r_{yy}/B = 0.24. $t = 0$ corresponds to start of the wave-maker. Using wave group velocity C_g predicted by linear wave theory, t_1 refers to the time that reflections from the model reach wave probe 1, and t_2 refers to the time when re-reflections from the wave-maker reaches the model. The RAOs are obtained from average amplitudes of the near steady part of each time-series as indicated in the figure.

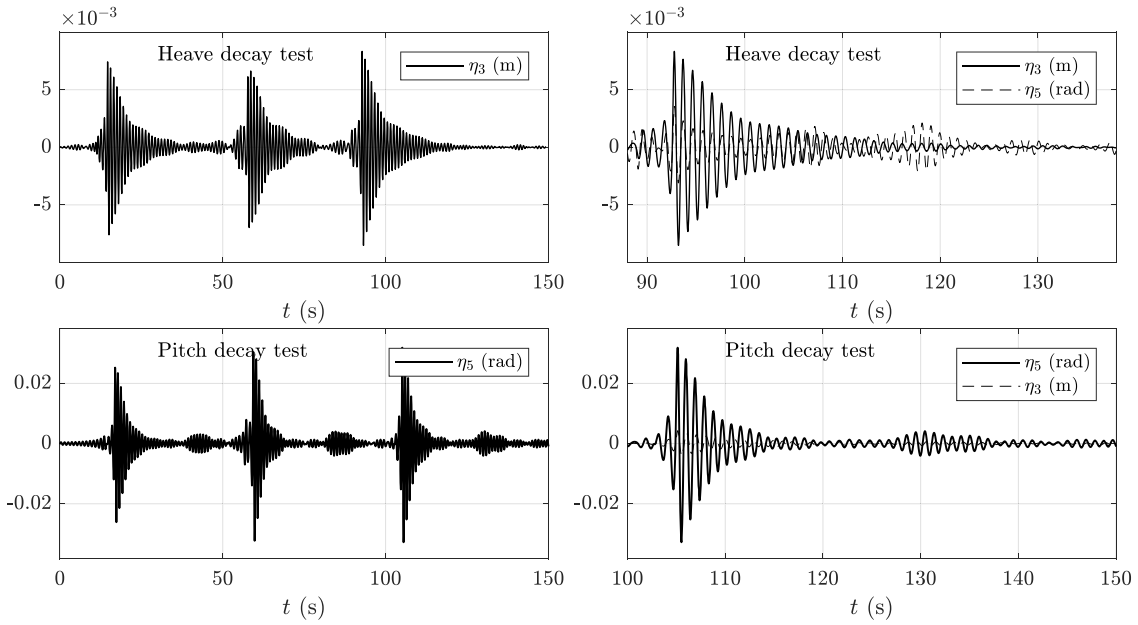

Fig. 5. Results from heave and pitch decay tests of the case with App2 moonpool inlet configuration, beam-to-draft ratio $B/D = 8.7$ and pitch radius of gyration $r_{yy}/B = 0.24$. Upper: heave decay tests. Lower: pitch decay tests.

maker ($L = 7.8$ m). For the wave periods close to resonance and cancellation, there were 20-25 wave periods until re-reflections. The effect of re-reflections are exemplified in Fig. 4 for wave period $T = 0.94$ s and wave steepness $H/\lambda = 1/60$. The chosen time-intervals used for extracting the response amplitudes are indicated by horizontal lines with triangular markers. There are clear wave reflections from the model back to wave probe 1 at time t_1. However, this does not (linearly) disturb the incident waves on the model. More importantly is the fact that there are also clear re-reflections from the wave-maker back to the model on the rigid body motions at time t_2. Although a near steady-state is reached, this represents an error source in our experiments. It appears that the heave motions are still increasing when the re-reflections occur, although it is not easy to judge, due to the beating type of behaviour which is present due to a set of closely spaced natural periods of the heave, pitch and piston-mode. Preferably, one would use a longer wave tank.

The presented time-series are representative for the freely floating tests. In the forced motion tests, arbitrarily long time-intervals of near steady-state wave elevations was achieved due to that the radiated waves were efficiently absorbed by the parabolic beaches.

Repetition tests were carried out. The results are presented later in the text (cf. Fig. 14). The standard deviations are in general within 3-4% of the mean values.

The forced motion amplitudes, η_{3a} and η_{5a}, as well as the incident wave amplitudes, ζ_a, were in general 2 - 10% lower than that prescribed. However, this is accounted for by non-dimensionalizing the RAOs with the measured, steady state amplitudes.

Investigation of video recordings did not indicate any significant three-dimensional disturbances. Wall gap effects have earlier been found to be minor in forced motion moonpool tests. Occasionally, the model was observed to nearly touch the glass walls of the wave flume. Damping of resonant pitch motions may therefore have been affected, but we have not been able to quantify this effect.

Ventilation around the lateral corners of the model at the highest wave period for wave steepness $H/\lambda = 1/30$ was observed. It is expected that this affected the body motions, but it was not investigated in detail. The numerical simulations were carried out only for the smallest wave steepness, $H/\lambda = 1/60$, and the wave periods of main interest was lower.

A small water leakage of about 3 mm during the first two days of the experiments led to some minor wave reflections for some tests, as well as a minor change of piston-mode natural frequency. The wave reflections appear as small irregularities in the free-surface RAOs for some tests. The beaches were carefully positioned such that the upper part was submerged by 1 mm. This has been found earlier to be important to efficiently damp out waves of very low steepness, such as those radiated from the present forced motion tests. The piston-mode resonance period was shifted by 1-2% for the affected tests due to a reduction in draft of 2-3%.

2.4. Data analysis

The results are in the present paper provided as non-dimensional responses; RAOs. The RAOs are computed from average amplitudes in near steady-state parts of the time-series, band-pass filtered around the basic harmonic. The time-windows were exemplified in Fig. 4 for wave period $T = 0.94$ s and wave steepness $H/\lambda = 1/60$. This corresponds to $T^* = 6.58$, where $T^* = T\sqrt{g/b}$ is the dimensionless period for which the results will be presented throughout the paper.

The free-surface RAO in forced heave motion cases is defined as ζ_g/η_{3a}, where ζ_g refers to the amplitude of the first harmonic of the wave gauges inside the moonpools, and η_{3a} refers to the amplitude of the first harmonic of the forced heave motion. Similarly, in the forced pitch motion cases, the free-surface RAO is defined as $\zeta_g/b'\eta_{5a}$, where b' is the distance from the model centre-line to the middle of the moonpool, and η_{5a} represents the amplitude of the first harmonic of the forced pitch motion. In this way, the free-surface motion is normalized by the mean local vertical body motion across the moonpool in the pitch case. In the freely floating tests, the free-surface RAOs are defined by ζ_g/ζ_a, where ζ_a is the amplitude of the first harmonic of the incident wave. The rigid body motion RAOs are defined as η_{3a}/ζ_a and $\eta_{5a}/k\zeta_a$, where k is the wave number.

All free-surface RAOs inside the moonpools are transferred to the Earth-fixed coordinate system by subtracting the vertical motion of the wave gauge from the measured free-surface elevation. The heave and pitch motions are obtained by integration of the accelerometer signals,

$$\ddot{\eta}_3 = \frac{a_{z1} + a_{z3}}{2}, \tag{1}$$

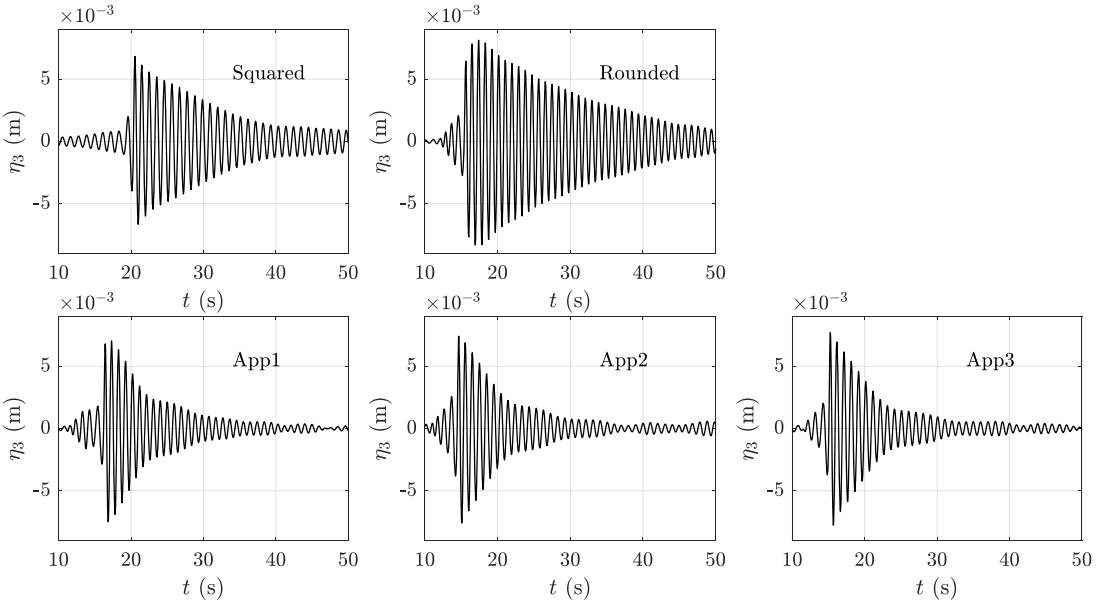

Fig. 6. Results from heave decay tests of all five moonpool inlet configurations, beam-to-draft ratio $B/D = 8.7$ and pitch radius of gyration $r_{yy}/B = 0.24$.

$$\ddot{\eta}_5 = \frac{a_{z1} - a_{z3}}{L_a}, \tag{2}$$

where $L_a = 1.2$ m is the center-to-center distance between the two accelerometers. The accelerometer signals were band-pass filtered in a narrow frequency range around the basic (wave) harmonic in order to avoid in particular low-frequency noise, and integration was performed in frequency domain.

2.5. Free decay tests

Free-decay tests of all geometric configurations were performed. An example is provided in Fig. 5 for the moonpool inlet with medium appendage (App2), and lowest radius of pitch gyration $r_{yy}/B = 0.24$. Three decays were performed for each, as illustrated in the left part of the figure. The last one is shown in more detail in the right part of the figure. The two upper figures represent the heave decay test. Due to that it is difficult in practice to achieve pure heave, also the pitch motion is provided in the top right figures. Similarly for pitch in the lower right figure.

We made an attempt to extract heave and pitch damping using logarithmic decay analysis. However, due to beating type of behaviour caused by the piston-mode resonance, there is no clear decay throughout the test. The time-series of the heave and pitch motions are not monotonically decaying, as exemplified around 100–105 s in the upper right figure. Even though a quantitative (logarithmic decay) analysis cannot therefore be performed, we observe that there are clearly different levels of damping between the five different inlet geometries. This is illustrated in Fig. 6. There are clear quantitative similarities between the three cases with appendages in the inlet. In the rounded inlet case, the system is clearly less damped as compared to the others. This illustrates that the damping in heave is clearly dependent on the energy dissipation due to flow separation at the moonpool inlet. Similar observations are made for pitch.

3. Numerical simulations

Numerical simulations were carried out for selected forced motion and freely floating cases. In the forced motion case, the two highest forcing amplitudes were simulated for the two cases with squared and largest appendage (App3) moonpool inlet configurations. In the freely floating case, only the square corner inlet configuration with the lowest radius of pitch gyration $r_{yy}/B = 0.24$ at the smallest wave steepness $H/\lambda = 1/60$ was simulated.

3.1. Forced motion simulations

The SINTEF Ocean (former MARINTEK) implemented software Potential Viscous Code (*PVC*) was used for the forced motion simulations. The code is based on the hybrid methodology coupling potential and viscous flow solvers developed by Kristiansen and Faltinsen (2012). The code has been used to study different two- and three-dimensional moonpool cases, see for instance (Kristiansen et al., 2013) and (Ommani et al., 2016b). The method involves a Navier Stokes solver with linearised free-surface and linearised or exact body-boundary conditions.

We emphasize that there is no empirical or artificial damping added in the simulations. The flow is solved for by first principles, i.e. by the Navier–Stokes solver; the main difference from a standard two-phase CFD analysis is that the free-surface conditions are linearized according to linear potential flow theory. This facilitates much larger cell size at the free surface, since the wave amplitude itself does not need to be resolved, only the wave length. Fast and robust computations are achieved in this manner. The method has proven very useful in marine resonance problems such as moonpool and roll resonance. CPU times of minutes, rather than hours or days are achieved in practice.

Linearised free-surface and body-boundary conditions have been found to be sufficient for moonpool resonance, as long as the relative velocity at separation points at the moonpool inlet is dominated by the water motion. The strength of the separating vortical structures is then well captured, and thereby the damping of the resonant piston-mode motion.

We emphasize that linearised body-boundary conditions are not applicable for vessel roll. There, the roll motion of the body is the main contributor to the relative water velocity at the bilges. It was shown in (Fredriksen et al., 2015) that linear body-boundary conditions are not sufficient to capture flow separation at the bilges. *PVC* has been further developed for vessel roll, cf. (Ommani et al., 2016a) and (Ommani et al., 2016c), where the main difference is that fully-nonlinear body--boundary conditions are applied in order to remedy this. This is achieved in their work by a deforming mesh technique.

In the case of forced heave, both linear and fully nonlinear body-boundary conditions (i.e. deforming mesh) were simulated in the

Table 3
Numerical mesh parameters for simulations with Potential Viscous Code (*PVC*). N means total number of cells. N_g means number of cells across the moonpool.

Mesh	N	N_g
Mesh 1	17 852	10
Mesh 2	20 158	20
Mesh 3	27 268	35
Mesh 4	50 058	70
Mesh 5	130 550	130

present study. Negligible differences in results were found. In the case of forced pitch motions, fully nonlinear body-boundary conditions were employed only.

A mesh size convergence study was performed using forced pitch motion of the square moonpool inlet as a test case. The results are presented in Fig. 7 in terms of moonpool free-surface RAOs. Mesh 3 (in the vicinity of the body) is illustrated in Fig. 8. The results are clearly sensitive to the mesh. According to our experience, the main physical feature to capture adequately for piston-mode resonance are the main vortical structures emanating from the moonpool inlets. Based on the results in Fig. 7, mesh 4 was selected. Although one cannot claim uniform convergence, it appears that the main physics is captured for the present cases with this mesh, since Mesh 4 and 5 give very similar results. A similar mesh convergence study was performed for forced heave, and the results were considerably less mesh-dependent. Pitch motions thus seems to be more sensitive, at least in the present set-up.

Running 40 forced oscillations with mesh 4, took typically about 120 s on a single processor using a regular laptop equipped with an Intel i7-5500U CPU with 8Gb RAM. The number of time-steps per oscillation was approximately 40. The method is thus very efficient, with the reason discussed above.

3.2. Freely floating body simulations

Solving for the equations of body motions is not implemented at present in *PVC*. Fredriksen's (Fredriksen et al., 2015) numerical code was used to simulate the freely floating body in waves. The code is based on a similar hybrid method as *PVC*, combining potential flow and Navier Stokes solvers. The difference is that this code employs fully nonlinear body-boundary conditions as well as fully nonlinear free-surface conditions, and the problem is solved in body-fixed coordinates. The main parameters of the mesh was similar to Mesh 4 above.

4. Theory

The most important mode in the moonpool in our case is the piston mode. When there are two moonpools, there are two piston modes; one when the two water columns oscillate with the same phase, and one when they oscillate with opposite phase. We refer to these two modes as symmetric and antisymmetric piston modes. In freely floating conditions, both piston modes will be excited and influence the body motions. Both modes are excited by the diffraction problem (body fixed in incident waves), whereas the symmetric piston mode is excited by heave motions only, while the antisymmetric piston mode is excited by pitch motions only.

We see from the forced motion tests that the two piston mode natural frequencies differ by about 6%. This is explained by that the moonpool flow will differ for the two modes. In the antisymmetric case, the two moonpool piston modes mutually excite each other, whereas in the symmetric case, the flow will be as if there is a vertical wall in the centerline of the model.

In order to investigate the differences, we developed a simplified analysis inspired by that of Molin (2001). He applied the matched eigenfunction expansion technique in order to approximately solve the spectral problem for a rectangular barge with one moonpool. In the

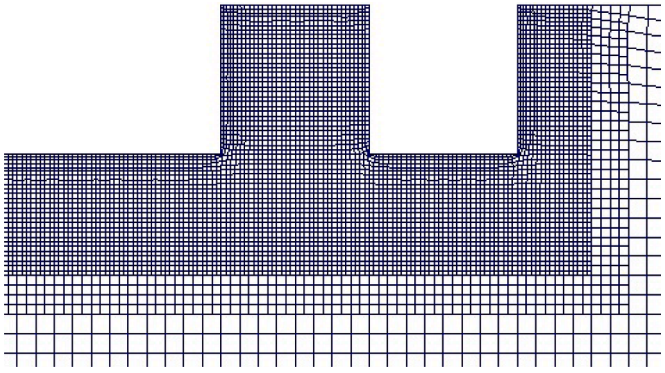

Fig. 8. Numerical mesh in the vicinity of the right moonpool, used in the forced heave and pitch motion simulations with Potential Viscous Code (*PVC*). Mesh resolution level 3, cf. Table 3 and Fig. 7.

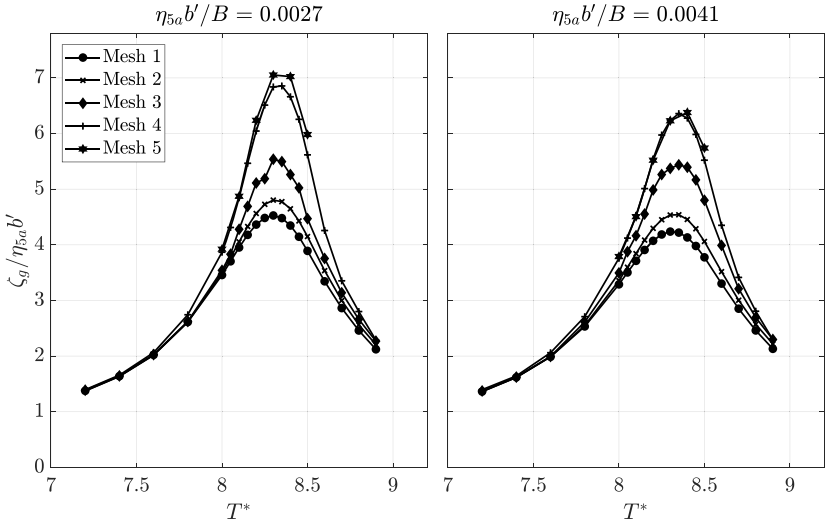

Fig. 7. Convergence study in terms of free-surface moonpool RAOs from forced pitch motion simulations with Potential Viscous Code (*PVC*). See Table 3 for mesh descriptions. The results are clearly mesh dependent. Mesh 4 was applied in the main analysis. The results were considerably less mesh dependent in forced heave simulations.

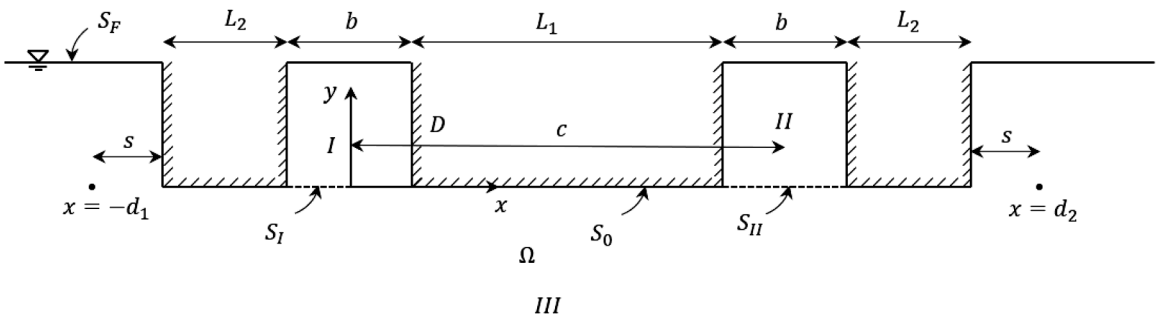

Fig. 9. Definitions of parameters used in the approximate solution of the spectral problem to predict the two piston-mode natural frequencies (symmetric and antisymmetric problems). Domains I and II are defined by the vertical moonpool walls, the free surface $y = D$ and the moonpool entrance $y = 0$. Domain III constitutes the remaining part of the fluid domain Ω. S_0 is the boundary of the total body.

two-dimensional case he represented the flow to both sides of the body by two sources (sinks).

We assume that the fluid is inviscid and incompressible, and that the flow is irrotational. We may then use potential flow theory. The spectral problem involves solving a linearised potential flow boundary-value problem with zero Neumann conditions on the body boundaries, in order to find natural frequencies ω. We define a Cartesian coordinate system $0xy$ with the vertical y-axis pointing upwards and with origin in the centre-line of the inlet of moonpool I, see Fig. 9. The free surface is located at $y = D$ and denoted by S_F (including the free surface both in the moonpools and exterior of the body). The water domain is denoted Ω, where domains I and II represent the moonpools and domain III the remaining part of the domain. The body surface (including all three hulls) is denoted S_0. Harmonically oscillating conditions are assumed such that the velocity potential may be expressed as $\Phi(x,y,t) = \Re(\varphi(x,y)e^{-i\omega t})$. The spectral problem for φ is

$$\nabla^2\varphi = 0 \quad \text{in } \Omega \tag{4}$$

$$\frac{\partial\varphi}{\partial n} = 0 \quad \text{on } S_0 \tag{5}$$

$$-\omega^2\varphi + g\frac{\partial\varphi}{\partial y} = 0 \quad \text{on } S_F \tag{6}$$

$$\varphi \to 0 \quad \text{as } r \to \infty \tag{7}$$

Here, $\partial/\partial n$ denotes normal derivative and $r = \sqrt{x^2+y^2}$.

We solve the spectral problem (4–7) approximately. The approximation lies in that the domain exterior to the body is represented by point sources located some distance away from the lateral bilges, at $x = -d_1$ and $x = d_2$, $y = 0$. This approach was cleverly suggested and used by Molin (2001). Further, we assume that the two moonpools are sufficiently far away from each other such that the influence of moonpool II on moonpool I can be represented by a point source located at the middle of moonpool entrance II. The free-surface conditions are satisfied only in the moonpools. The flow to the sides of the body is not physical.

It is sufficient to perform the matching at the entrance of moonpool I only, denoted S_I, (or equivalently, at the entrance of moonpool II only). The matching involves requiring equality of the normal velocity; $\partial\varphi_{III}/\partial y = \partial\varphi_I/\partial y$ on S_I and equality of pressure (velocity potential) on average over S_I.

In our analysis we keep only the lowest order terms of the eigenfunction expansion in the moonpools;

$$\varphi_I = A_0 + B_0\, y/D, \tag{8}$$

meaning that the flow is uniform and vertical in the moonpools. The zero Neumann condition along the vertical moonpool walls is satisfied with this solution.

In the symmetric problem, we require that $\varphi_{II} = \varphi_I$, while in the antisymmetric problem we require $\varphi_{II} = -\varphi_I$. Placing all sources and source distributions at $y = 0$ satisfies the zero Neumann body-boundary condition along the bottom of the hull, at $y = 0$.

The solution of the velocity potential in domain III (below the body) is now, for the symmetric problem,

$$\varphi_{III}(x, y=0) = -\frac{1}{\pi}\int_{S_I}\frac{B_0}{D}[\log|x-\xi| - \log|x+d_1| - \log|x-d_2| + \log|x-c|]\mathrm{d}\xi. \tag{9}$$

Here, we have applied continuity of normal velocity along S_I by means of using the moonpool (piston-mode) velocity $\frac{\partial\varphi_I}{\partial y} = B_0/D$ at $y = 0$. The point sources outside the body are necessary in the symmetric problem in order for the potential (and pressure) to vanish at infinity; their strengths are equal to each of the two moonpools, with opposite sign. This is different to Molin, where each source has half the source strength of the moonpool in order to achieve balance. While the vertical position is given as $y = 0$ in order for the zero normal flow body-boundary condition on the bottom of the body to be satisfied, the horizontal coordinate is not uniquely given. Molin argued that the position should be a small distance away from the barge keel.

In the antisymmetric problem, the lateral point sources are not strictly speaking necessary, since the two moonpools act as a source and a sink with equal strength, and therefore in total vanish at infinity. However, neglecting these implies that all the flow must go from one moonpool to the other. There will certainly also be some flow communicating with the exterior domain, and so, they should be included. The weight, say β, of the point sources are unknown, however, so we must make a qualified guess. We suggest a simple geometric weighting, $\beta = c/(c+d_1)$. c is the center-to-center distance between the two moonpools, and d_1 is the distance from the center of moonpool I to the left point source. We then have for the antisymmetric problem,

$$\varphi_{III}(x, y=0) = -\frac{1}{\pi}\int_{S_I}\frac{B_0}{D}[\log|x-\xi| - \beta\log|x+d_1| + \beta\log|x-d_2| - \log|x-c|]\mathrm{d}\xi. \tag{10}$$

We now assume that $b/2$ is small compared to c, d_1 and d_2. We may then simplify the three point source terms to $\log\gamma$, where $\gamma = c/d_1d_2$ in the symmetric problem and $\gamma = c^{-1}(d_2/d_1)^\beta$ in the antisymmetric problem. The theory may be generalised to several moonpools, as long as they are some distance apart so that they may be assumed to be in each other's far field. The only consequence of more than two moonpools is more factors in γ. A relevant theory was developed by Miles (2002). He investigated a three-dimensional body of infinite horizontal extent, with arbitrary number of moonpools with circular cross-section.

The matching of the pressure in an average sense involves integration over S_I,

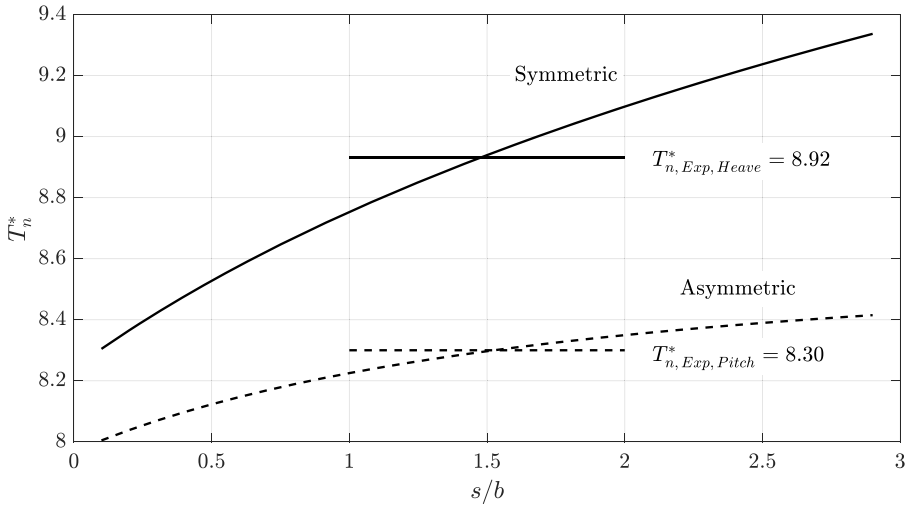

Fig. 10. Curves represent natural periods predicted by the presented approximate theory of the symmetric and antisymmetric problems as function of the non-dimensional position of the laterally placed sources, s/b. $T^* = T\sqrt{g/b}$. The experimentally obtained piston-mode periods from forced heave (symmetric) and forced pitch (antisymmetric) tests are indicated by the horizontal lines. In both the symmetric and antisymmetric cases the experimentally obtained natural piston modes indicate that the position of the lateral sources are as much as $s = 1.5b$ from the latereal bilges of the body.

$$\int_{S_I} \varphi_I \, \mathrm{d}x = \int_{S_I} \varphi_{III} \, \mathrm{d}x. \tag{11}$$

Inserting (8) and (9) or (10) into the matching condition (11) results in a double integral on the right hand side of (11). This gives us

$$A_0 \Big/ B_0 = \frac{b}{\pi D}\left(\frac{3}{2} - \log b\gamma\right). \tag{12}$$

The free-surface condition $-\omega^2\varphi_I + g\,\partial\varphi_I/\partial z = 0$ on $z = D$ gives the relation

$$\omega^2 = \frac{g}{D(1 + A_0/B_0)}. \tag{13}$$

Inserting (12) into (13) gives the natural piston-mode frequency as

$$\omega^2 = \frac{g}{D\left(1 + \frac{b}{\pi D}\left(\frac{3}{2} - \log b\gamma\right)\right)}. \tag{14}$$

Numerical values of the natural periods, T^*_n, as function of the distance from the lateral bilges of the body to the sources/sinks normalized by the moonpool width, s/b, are provided in Fig. 10. The draft is $B/D = 6.5$, and the other geometrical parameters are as those in the experiments. The experimentally obtained natural periods from the forced heave and pitch tests (to be presented later) are indicated by horizontal lines. The best agreement between the theory and the experiments appears for $s/b \simeq 1.5$. This is a reasonable position seen from a physical point of view. More important than the exact position of the lateral sources is that the simplified theory qualitatively predicts that the natural period of the symmetric problem is higher than that in the antisymmetric problem, which is consistent with the experimental results. It is consistent with our intuition that the water will flow with more ease when it may (partly) flow back and forth between the moonpools as it may in the antisymmetric problem, and not only towards the lateral sides of the body as it must in the symmetric problem, and this will result in a higher natural frequency.

The real problem involves a freely floating body, and not forced motion. The lateral sources will also have consequences for the pitch *response* in freely floating conditions, as the flow due to the piston-mode underneath the lateral part of the body will considerably influence the hydrodynamic pitch moments, and play a major part in the coupled pitch/piston mode system. More work would be needed in order to develop an approximate theory for the freely floating problem due to the difficulties with solving the radiation problem in an approximate manner. An eigenvalue problem of the freely floating case using added mass coefficients extracted from forced motion time-domain simulations with PVC is presented in the last part of the paper.

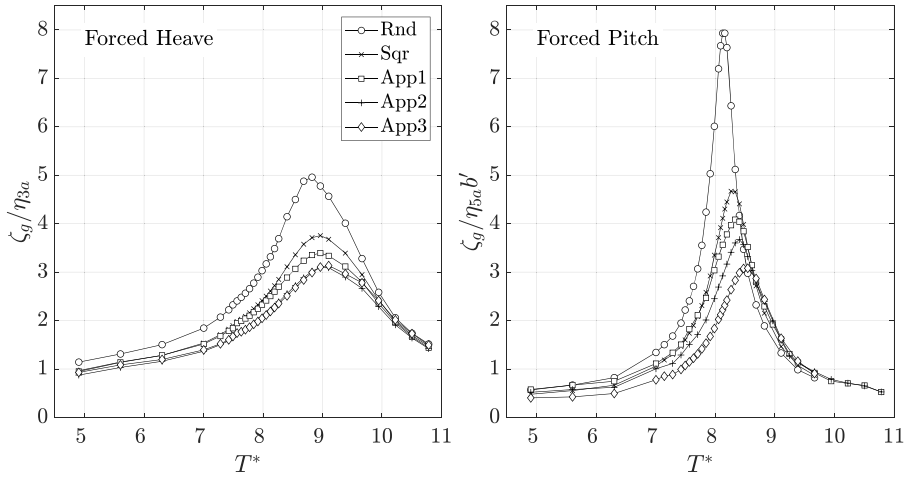

Fig. 11. Experimental piston-mode RAOs from forced motion tests illustrating the effect of the five different moonpool inlet geometries. The RAOs are average values of the moonpool wave gauges wp 2-5. Largest forced motion amplitudes $\eta_{3a}/B = 0.0058$ and $b'\eta_{5a}/B = 0.0041$. $b' = 0.350$ m is the distance from the model centre to the centre of the moonpools, cf. Table 1. Draft $B/D = 6.5$.

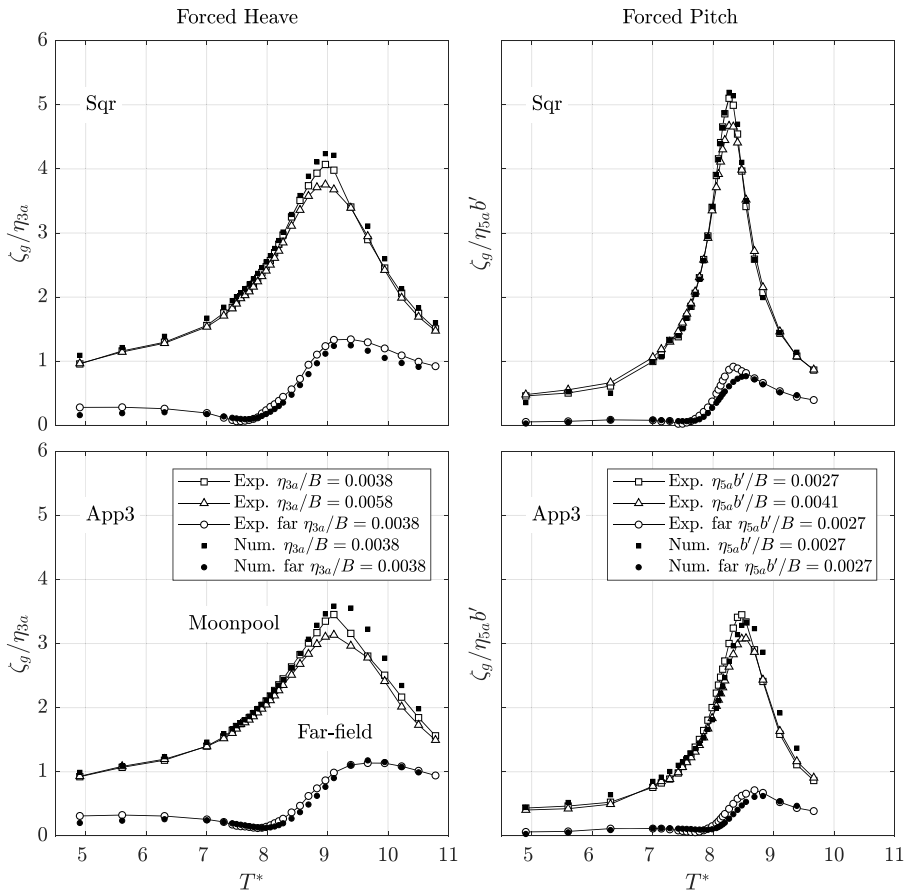

Fig. 12. Numerical versus experimental moonpool RAOs for the cases with square moonpool inlets and the largest appendage moonpool inlet (App3) configurations for the forced motion tests. Left: forced heave. Right: forced pitch. From the experiments, the two largest forcing amplitudes are included. The effect of forcing amplitude is small. The data points indicated as Far-field refer to wave probe 7, 1 m from the hull. $B/D = 6.5$.

5. Results

We first present and discuss results from the forced motion case, and next the freely floating case. We last perform an eigenvalue analysis of the freely floating case.

5.1. Forced heave and pitch

Earth-fixed moonpool RAOs for the five different inlet configurations are presented in Fig. 11 under forced heave and forced pitch, for the largest forcing amplitude. As discussed above, the natural periods in the forced heave (symmetric) and forced pitch (antisymmetric) problems differ. For instance, the natural period in forced heave is about 6% higher than that in forced pitch in the case with square moonpool inlet geometry. In forced pitch, the two moonpools mutually excite each other, whereas, in forced heave, they do not. As a result, not only the natural periods differ, but the moonpool response is in general larger in forced pitch than forced heave, as seen from the experimental results.

The largest appendage moonpool inlet (App3) causes smallest resonant responses, whereas the rounded inlet the largest. The fact that the largest inlet causes smallest moonpool response may be anticipated due to larger damping caused by the strong geometric singularities at the moonpool inlet (the lower end of the vertical plates at the moonpool entrance). It is also anticipated that the response is largest for the rounded inlet case, since there should have been negligible damping due to none, or very weak flow separation in the present small Keulegan Carpenter (KC) number range. We use KC $= w\,T_g/d$ as a measure of the KC number, where T_g is the natural piston-mode period, $w = \omega_g\zeta_g$ is the amplitude of the vertical velocity of the piston-mode free-surface at resonance frequency $\omega_g = 2\pi/T_g$ and $d = 2r = 2\times 0.04\text{m} = 0.08$ m is two times the radius of the moonpool inlet (cf. Fig. 3). The largest KC number in the forced heave tests is then 4.7, for $\eta_{3a} = 0.0075$ m amplitude and moonpool RAO of 5. The largest KC number in the forced pitch tests is 4.2, for local heave amplitude in the moonpool $b'\eta_{5a} = 0.0053$ m and moonpool RAO of 8. Flow over a blunt body (like the rounded moonpool inlet) at KC numbers of 4-5 indicates minor flow separation effects. This is supported by that the rounded inlet moonpool RAOs from the tests with small and medium forcing amplitudes (not shown) are practically identical to the ones presented in the figure for the largest forcing amplitude.

An increased resonance period for appendages, relative to square moonpool inlet, is explained by that they represent an increased effective draft. This results in a larger effective piston-mode mass. Both the effect of reduced piston-mode response and shift in natural period may be exploited in a design. In particular, we expected a priori that a reduced piston-mode response would be beneficial for the performance of the bridge foundation. However, as discussed later in the paper, the rounded and square moonpool inlets seem to out-perform the inlets with vertical plates in that they provide a higher degree of pitch reduction.

Experimental and numerical RAOs are compared in Fig. 12 for square inlet and largest appendage case (App3), both for forced heave and forced pitch, for the medium and large forcing amplitudes. The draft is $B/D = 6.5$. The numerical results are averaged free-surface elevation across the moonpool, and the experimental are averaged values of the two moonpool wave gauges. The agreement between the experiments and simulations is in general satisfactory. This provides confidence in the experiments, as well as validation data for the numerical simulations. We would like to point out that, despite the numerical difficulties

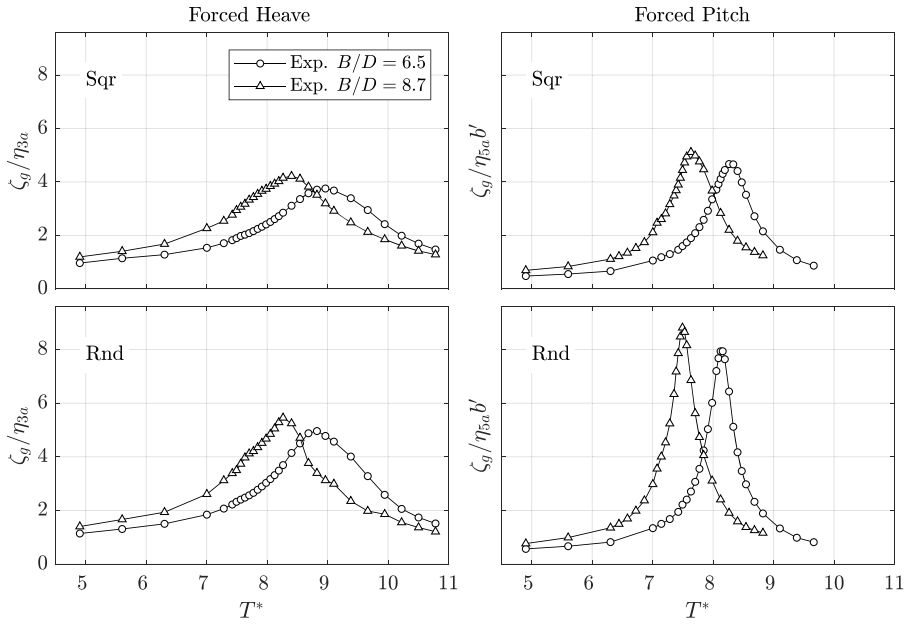

Fig. 13. Experimental moonpool RAOs for square and rounded moonpool inlets illustrating the effect of changing the draft. Upper: square moonpool inlet. Lower: rounded. Largest forced motion amplitudes ($\eta_{3a}/B = 0.0058$ and $b'\eta_{5a}/B = 0.0041$).

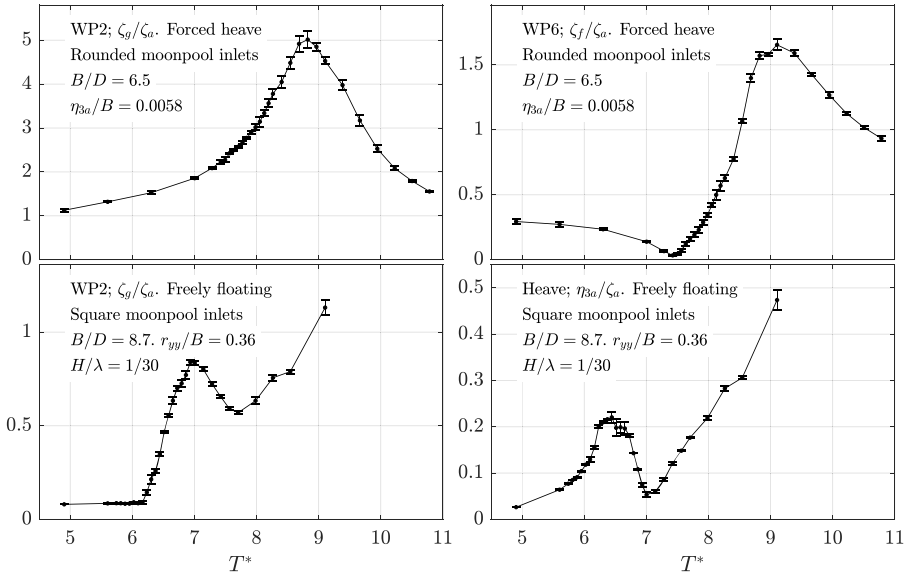

Fig. 14. Mean and standard deviations of selected, representative responses obtained from the repetitions tests. The analysis is based on five repetition tests in all the cases. Upper: forced motion. Lower: freely floating tests. The standard deviation is in general within 3-4% of the mean values.

experienced in general with flow of a viscous fluid across flat plates, the *PVC* simulations are able to predict the moonpool response well also for the App3 geometry.

The effect of motion amplitude is not pronounced for the present square moonpool inlet set-up. It is in general more pronounced with smaller ratios between moonpool gap width and body beam, cf. for instance (Faltinsen et al., 2007). The reason is that, in our case, wave radiation damping (of the piston-mode) dominates over that due to flow separation. If the moonpool width, b, is reduced relative to the body beam, B, or the moonpools are placed closer to the middle of the body, higher resonant piston-mode response is expected, leading to more relative importance of flow separation damping, and therefore amplitude-dependent RAOs.

The effect of changing draft is mainly that of a shift in the piston-mode period, as expected. This is illustrated in Fig. 13. Experimental results for square and rounded inlets are presented, for the highest forcing amplitude. The response is observed to be somewhat larger for the smallest draft. This is in fact opposite to what was observed by Fredriksen et al. (2014) in their forced heave tests of a body with a single moonpool.

Results from the repetition study are presented in Fig. 14. The two upper plots represent forced motion tests, while the two lower plots freely floating tests. The results are based on five repetitions. Mean values of selected responses are presented, accompanied by the standard deviation. The standard deviation provides a measure of the random errors. Around the resonance peaks, the standard deviation relative to the mean is in general within 3-4%, and we conclude that the degree of repeatability is within typical experimental error levels.

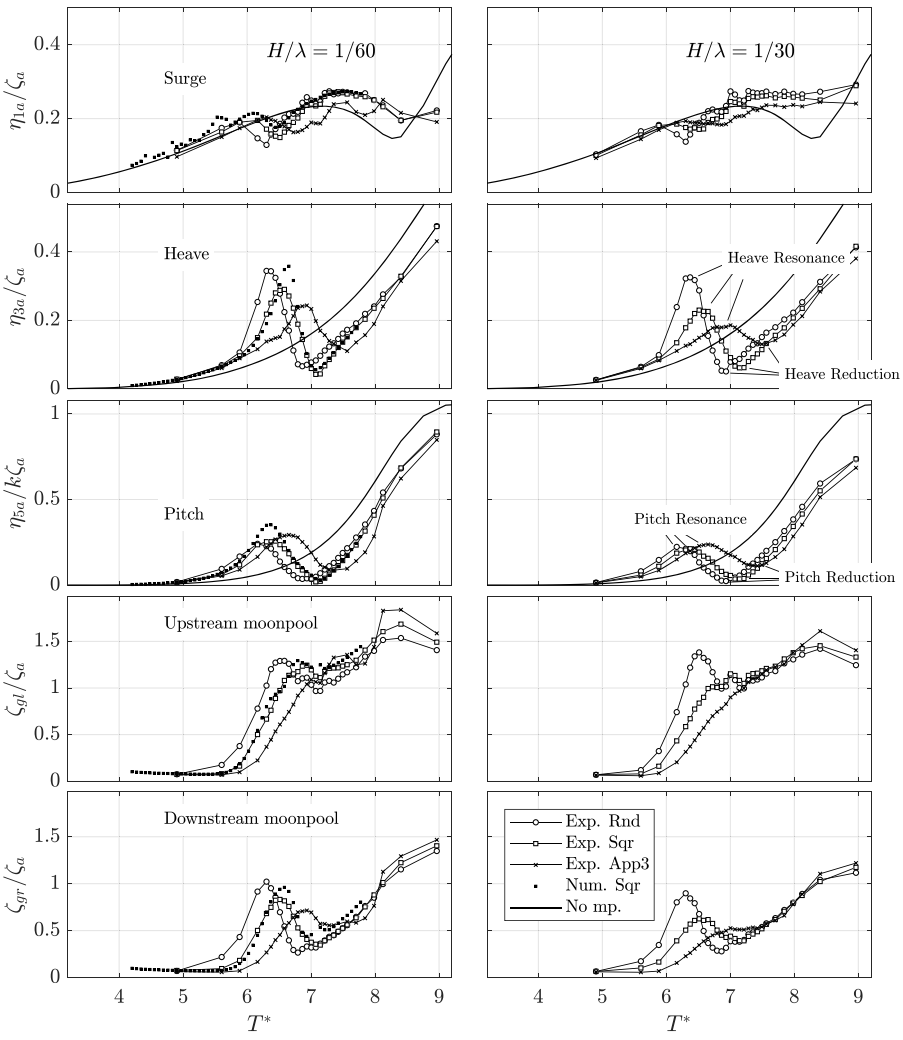

Fig. 15. Experimental and numerical RAOs obtained from the freely floating cases in waves. From top to bottom: surge, heave, pitch and moonpool RAOs. Lowest radius of gyration $r_{yy}/B = 0.24$. Draft $B/D = 8.7$. The resonance peaks in heave and pitch, as well as period intervals with heave and pitch reduction (near cancellation) are indicated. The curves denoted by "No mp." in the legend refers to 2D potential flow theory computations of a barge without moonpool with the same width B, draft D and radius of pitch gyration I_{55} as the model with moonpool.

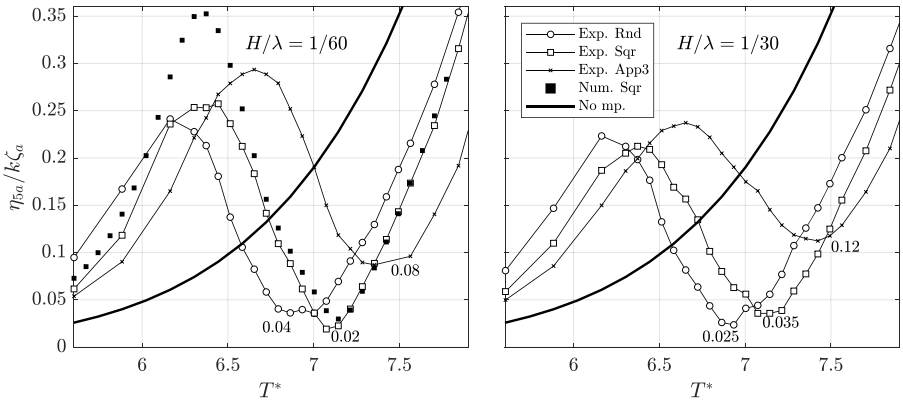

Fig. 16. Focused view of the pitch RAOs from the freely floating tests provided in Fig. 15. The values of the RAOs at the local minima denoted "Pitch reduction" in Fig. 15 are provided. The square and rounded moonpool inlets provide the best pitch reduction with pitch RAO between 0.02 and 0.04, depending on the inlet geometry and wave steepness. The largest appendage inlet (App3) provides less good pitch reduction (RAOs between 0.08 and 0.12), and increasingly less good with increasing wave steepness.

5.2. Freely floating model in waves

Experimental and numerical RAOs for surge, heave and pitch motions, and free surface inside the two moonpools are provided in Figs. 15 and 16 for two wave steepnesses ($H/\lambda = 1/60$ and 1 /30). The beam-to-draft ratio is $B/D = 8.7$. The latter figure represents a focused view of the pitch RAO in the most interesting wave period range, i.e. the wave period range including pitch resonance and near-cancellation, for increased clarity. η_1, η_3 and η_5 refer to surge, heave and pitch motion, respectively. ζ_{gl} and ζ_{gr} refer to the upstream and downstream moonpools, respectively. The results denoted "No mp." in the legends refer to numerical simulations based on linearized potential flow theory for a barge with the same beam and draft as the studied model ($B = 1.3$ m and $B/D = 8.7$), but without moonpool. The same moment of inertia is used as in the experiments and other numerical simulations. The results do not include the two smallest appendages for clarity. The RAOs for these are in-between those for the square inlet and App3 inlet.

The main observation is that there are (desired) near-cancellation

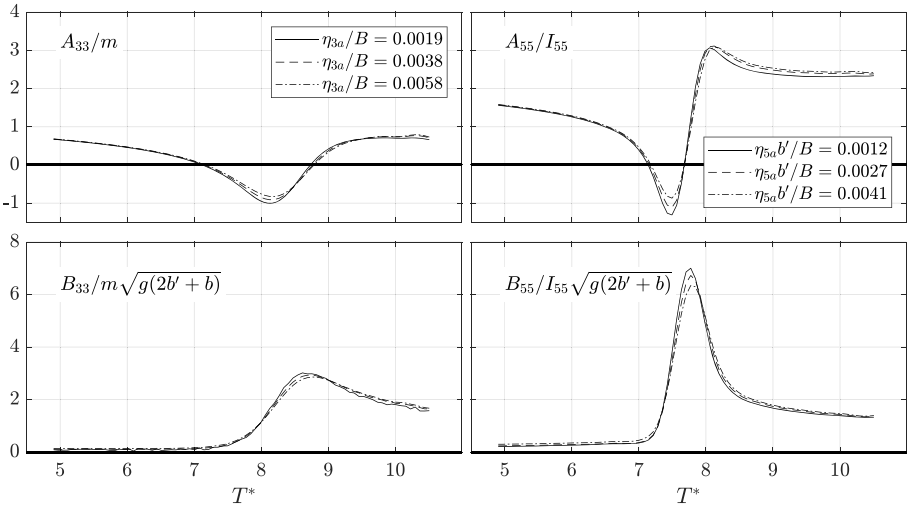

Fig. 17. Added mass and damping coefficients as calculated by the numerical code *PVC* for three different forcing amplitudes. Square moonpool inlets. Draft $B/D = 8.7$.

periods, as well as (undesired) resonance peaks in both heave and pitch. This is indicated by text in the right part of Fig. 15 as "Heave and Pitch Resonance and Reduction". In period ranges around the cancellation and resonance periods, the heave and pitch responses are clearly lower and higher than that of the barge without moonpool, respectively.

The resonance and (near) cancellation of heave and pitch are clearly correlated with resonant piston-mode motion in the two moonpools, and in particular the downstream moonpool. This illustrates that there is a strong coupling between the piston-modes and the heave and pitch motions. The resonance and cancellation frequencies for pitch, heave and moonpool differ slightly. This is explained by means of an eigenvalue analysis in the last part of the paper. There is an inertial coupling between surge and pitch, while heave is (linearly) de-coupled due to symmetry of the body around $x = 0$. However, there will be a nonlinear coupling between heave and pitch due to flow separation.

The numerical results are in overall fair agreement with the experimental values. We emphasize that the numerical simulations are performed by a Navier–Stokes solver, so there is no empirical or artificial damping added. The overall fair agreement provides further confidence in both experiments and numerical schemes. One exception is that the numerical simulations over-predict in the order of 20% at heave and pitch resonance. As mentioned earlier, some contact between the model and the glass wall of the tank occurred, something which may have caused additional damping.

The values of the pitch RAOs at the local minima (near-cancellation period), are provided by text in Fig. 16. The RAO values are here as low as 0.02 and 0.04 for the rounded and square inlet geometries. The rounded and square moonpool inlets show opposite trends with respect to wave steepness. The corresponding numbers for the case of largest appendage inlet are 0.08 and 0.12, a factor 3-4 times higher than for rounded and square moonpool inlets. There is thus significantly less pitch reduction when inlet plates are added. Some of this effect might be due to potential flow effects, since the plates effectively "block" the communication between the two moonpools to some extent. However, the 50% increase from 0.08 at $H/\lambda = 1/60$ to 0.12 at $H/\lambda = 1/30$ indicates major contributions from flow separation at the plate ends. One would have hoped for that the flow separation effects could broaden the period range for which pitch reduction (near cancellation) is experienced. On the contrary, the present results show that they have an *unwanted* effect on the performance of the structure; the pitch motion is larger, and the period range for which there is a reduced pitch motion is not notably increased.

The pitch resonance peak is similar for the three moonpool inlet geometries, although the largest appendage moonpool inlet in fact provides inferior results, i.e. higher values of the pitch RAO at the resonance peak. For heave, however, the largest appendage case gives lower resonance peaks (Fig. 15). This is also the case for the downstream moonpool, although the moonpool responses are so moderate that they hardly pose a concern. There is considerably less moonpool response in the freely floating case than for forced motion. This is consistent with previous investigations in the literature, and related to phasing between the piston-mode excitation from heave motions, pitch motions and incident waves.

We deduce from this that *rounded and square moonpool inlets are most efficient for pitch reduction purpose*. The success in a practical design depends on the width of the response curve of the super-structure at its main resonant mode, how well the near pitch cancellation period of the floater is tuned to this, and the closeness of other resonant modes of the super-structure to the resonance peak introduced by the moonpools.

5.3. Eigenvalue analysis

The natural periods are studied by means of an eigenvalue analysis following that described in (Fredriksen et al., 2014). The square moonpool inlet case is chosen. The undamped and unforced equations of motion for the coupled three-degree of freedom system of surge, heave and pitch is analysed,

$$(M + A_{11})\ddot{\eta}_1 + (I_{15} + A_{15})\ddot{\eta}_5 + C_{11}\eta_1 = 0, \tag{15}$$

$$M\ddot{\eta}_3 + C_{33}\eta_3 = 0, \tag{16}$$

$$(I_{55} + A_{55})\ddot{\eta}_5 + (I_{51} + A_{51})\ddot{\eta}_1 + C_{55}\eta_5 = 0. \tag{17}$$

The quantities are referring to the coordinate system specified in Fig. 1. The restoring coefficient in surge, C_{11}, is given by the (soft) mooring line stiffness. Added mass coefficients are calculated from Fourier averaging of the force- and moment time-series obtained from the forced motion simulations using *PVC*. A_{33} and A_{55} are presented in the upper part of Fig. 17. The numerical results for $A_{35} = A_{53}$ (not presented) confirm that the coupling terms are zero, due to body symmetry. In reality, a small non-linear coupling is expected through the fact that flow separation at the moonpool inlets depend on the *relative* flow velocity, which in the freely floating case is a function of all rigid body modes. This is not included in this eigenvalue analysis. The added mass in heave and pitch are negative for period range close to the piston-mode natural period ($T^* = 8.3$), something which is a well-known feature in gap resonance problems. Results from the three simulated forcing amplitudes are

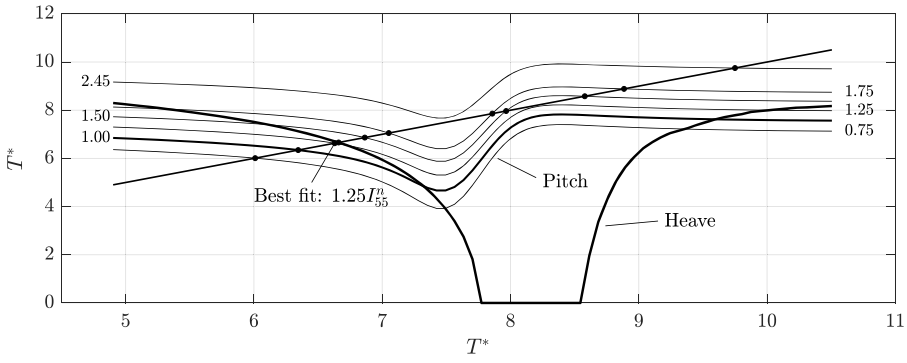

Fig. 18. Results from the eigenvalue analysis used to investigate the natural periods in heave and pitch. The natural periods are those where the curves intersect with the straight line $T^* = T^*$. The numbers indicate different moment of inertia I_{55} between $0.75I_{55}^n$ and $1.75I_{55}^n$. $2.45\,I_{55}^n$ refers to the tested model with the highest moment of inertia. Heave is de-coupled from the coupled surge-pitch motion, and therefore independent of I_{55}. By the marker "best fit" we refer to the simulations with best fit of the natural period peaks in the experiments in Fig. 19. The curve for surge is outside the vertical limit of the figure (the values are between 60 and 65 over the considered range of periods). Some curves intersect T^* three places, indicating three natural periods. The two highest natural periods are near critically or over-damped (see Table 4).

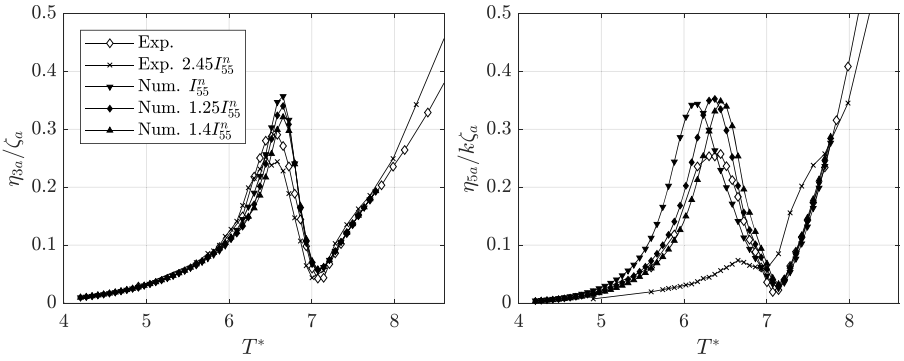

Fig. 19. Sensitivity of the heave and pitch RAOs to variation of the radius of gyration in pitch, I_{55}. I_{55}^n means the nominal value as found experimentally. The simulations with $I_{55} = 1.25I_{55}^n$ is clearly in best agreement with the experiments. The legend "Exp. $2.45I_{55}^n$" refers to the experimental case with the highest pitch radius of gyration (cf. Table 2). Square moonpool inlets.

included. The added mass coefficients are slightly amplitude-dependent, most notably around the natural piston-mode period. The values from the smallest forcing amplitude is used for the eigenvalue analysis.

Steady-state solutions are assumed, such that each motion is assumed to oscillate with frequency ω. The determinant of the resulting system matrix must be zero in order for the system to have non-trivial solutions. The solutions to natural frequencies are provided in the following manner. In Fig. 18, the natural periods are those where the different curves intersect with the straight, dashed line. The intersections are indicated by black dot markers. The curve for surge is outside the vertical limit of the figure, with values between 60 and 65 over the considered range of periods. The surge natural period is as high as $T_{n1}^* = 36.4$, due to soft mooring system.

The natural period in heave predicted by the eigenvalue analysis presented in Fig. 18 correspond well with that predicted by both experiments and numerical simulations; from the resonance peaks in Figs. 15 and 16, the heave resonance period for square moonpool inlet is $T^* = 6.55$, and the heave curve of Fig. 18 crosses the straight line at $T^* = 6.66$. This gives a discrepency of 1.5%; a quite fair comparison.

There are several curves representing pitch. The different curves correspond to different values of pitch moment of inertia, I_{55}. The thick curve corresponds to the nominal value, I_{55}^n, i.e. the value that was computed by summation of weights as given in Table 2. The other curves correspond to 0.75, 1.25, 1.50 and 1.75 times the nominal value. We can compare these results with the results from the numerical simulation sensitivity study presented in Fig. 19. The pitch natural period is in general predicted to be higher by the eigenvalue analysis than by the numerical simulations. For the cases with nominal and 1.25 times the nominal value, the eigenvalue analysis predicts 3.5% and 4.7% higher natural period, respectively.

Although the eigenvalue analysis is not highly accurate in predicting the natural periods, it does give interesting information regarding the existence of multiple natural periods. Two of the curves in Fig. 18 intersect the straight curve at three values of T^*. This indicates three resonance periods. The level of (resonant) response is then a matter of damping. Although the surge and pitch motions are coupled, we present in Table 4 the ratio between the actual pitch damping and critical pitch damping as though pitch was independent; $\xi_i = B_{55}(\omega_i)/2\sqrt{(I_{55} + A_{55}(\omega_i))C_{55}}$, since this will give a reasonable qualitative measure of the damping in pitch. $B_{55}(\omega_i)$ are taken from the PVC simulations, as presented in Fig. 17. The index $i = 1, 2$ or 3 refers to the crossing points in Fig. 18 numbered from left to right. We see from Fig. 15 that the resonance peaks of the RAOs all appear for crossing point 1 in Fig. 18. This is consistent with that ξ_1 is in the range $\xi_1 \simeq 0.12 - 0.3$, cf. Table 4, which means the system is not lightly damped, but far from critically damped. On the other hand, $\xi_2 > 1$, meaning the system is

Table 4
Ratio of actual damping to critical damping, ξ_i, relevant for the sensitivity analysis of natural periods of the coupled heave and pitch system (cf. Fig. 18). I_{55}^n refers to the nominal value of the pitch moment of inertia provided in Table 2.

I_{55}	ξ_1	ξ_2	ξ_3
0.75 I_{55}^n	0.13	-	-
1.00 I_{55}^n	0.14	-	-
1.25 I_{55}^n	0.15	-	-
1.50 I_{55}^n	0.17	1.71	0.87
1.75 I_{55}^n	0.29	3.40	0.71
2.45 I_{55}^n	0.27	3.29	0.61

over-damped at these periods, and there will be no resonant motion. For the third and highest natural period, however, ξ_3 is between 0.6 and 0.9, so one must expect undesired resonant motion also at this wave period, something which should be considered in design.

The experimental pitch RAO for the case with the highest radius of gyration, $2.45I_{55}^{n}$ (or $r_{yy}/B = 0.36$) is also included in Fig. 19. There is no resonance peak in the considered period range. This is consistent with the eigenvalue analysis (Fig. 18), which predicts a resonance at $T^{*} = 9.7$, which is outside the tested period range. The pitch response is quite low for this configuration, something we in fact seek in the present study. However, the pitch response is not as low as for the other radius of gyration case ($r_{yy}/B = 0.24$) around the near cancellation period $T^{*} = 7.2$. Also, it is a question whether a radius of gyration this high ($r_{yy}/B = 0.36$) is physically realisable from a structural point of view.

6. Concluding remarks

In the present paper we investigated a rectangular barge with two moonpools in a two-dimensional setting, by means of experiements, numerical simulations and theoretical work. The body was studied in both freely floating regular wave conditions, as well as forced heave and forced pitch. A main objective of the work was to assess different moonpool inlet configurations, and their efficiency to achieve (near) pitch motion cancellation. Five moonpool inlet configurations were investigated: rounded, square and square with three different size vertical plates extending below the moonpool inlets.

We found that the effect of flow separation at the moonpool inlets (which provide desired and dominant part of damping for the traditional moonpool problem), represents an *undesired* effect in the pitch cancellation problem; the pitch cancellation ability is significantly less for the configurations with vertical plates at the inlets relative to the configurations with rounded and square moonpool inlets. The moonpool responses were moderate, and should not pose a concern in practice. Based on this, square or rounded moonpool inlets were clearly found to best fulfil its purpose as pitch reduction device. A negative side effect of the moonpools is pitch and heave resonance in a period range close to the cancellation period. This increases the heave and pitch motions relative to a corresponding body with no moonpools. The vertical plate configurations gave, in addition to less efficient pitch cancellation, also slightly higher resonant pitch motion compared to the configurations with rounded and square moonpool inlet.

CRediT authorship contribution statement

Lars Mikkel Utnes Reiersen: Conceptualization, Formal analysis. **Trygve Kristiansen:** Conceptualization. **Babak Ommani:** Conceptualization. **Arnt Fredriksen:** Conceptualization.

Declaration of Competing Interest

The authors declare that there is no competing interest connected to the present manuscript. The manuscript, or versions of it, has not been submitted to other journals/conferences. There is no conflict of interest with other parts.

Acknowledgements

This work was partly supported financially by Multiconsult and partly supported by the Research Council of Norway through the Centers of Excellence funding scheme AMOS, project number 223254.

References

Faltinsen, O.M., Rognebakke, O.F., Timokha, A.N., 2007. Two-dimensional resonant piston-like sloshing in a moonpool. Linear inviscid statement. J. Fluid Mech. 575, 359–397. https://doi.org/10.1017/S002211200600440X.

Fredriksen, A.G., Bonnemaire, B., Lie, H., Tan, X., 2016. Comparison of global responses of a 3-span floating suspension bridge with different floater concepts. OMAE2016, Busan, South Korea.

Fredriksen, A.G., Kristiansen, T., Faltinsen, O.M., 2014. Experimental and numerical investigation of wave resonance in moonpools at low forward speed. Appl. Ocean Res. 47, 28–46. https://doi.org/10.1016/j.apor.2014.03.005.

Fredriksen, A.G., Kristiansen, T., Faltinsen, O.M., 2015. Wave-induced response of a floating two-dimensional body with a moonpool. Philos. Trans. R. Soc.London A 373 (2033), 20140109. https://doi.org/10.1098/rsta.2014.0109.

Kristiansen, T., Faltinsen, O.M., 2012. Gap resonance analyzed by a new domain-decomposition method combining potential and viscous flow. Appl. Ocean Res. 34, 198–208. https://doi.org/10.1016/j.apor.2011.07.001.

Kristiansen, T., Faltinsen, O.M., 2015. Experimental and numerical study of an aquaculture net cage with floater in waves and current. J. Fluids Struct. 54, 1–26. https://doi.org/10.1016/j.jfluidstructs.2014.08.015.

Kristiansen, T., Sauder, T., Firoozkoohi, R., 2013. Validation of a hybrid code combining potential and viscous flow with application to {3D} moonpool. OMAE2013.

Maisondieu, C., Boulluec, M.L., 2001. Flow dynamics in a moon-pool. Experimental and numerical assessment. OMAE2001, Rio de Janeiro, Brazil.

Miles, J., 2002. On slow oscillations in coupled wells. J. Fluid Mech. 455, 283–287. https://doi.org/10.1017/S0022112001007212.G 0215

Molin, B., 2001. On the piston and sloshing modes in moonpools. J. Fluid Mech. 430, 27–50.

Ommani, B., Fonseca, N., Kristiansen, T., Hutchinson, C., Bakksjo, H., 2016. Bilge keel induced roll motions of an FPSO with sponsons. OMAE2016, Busan, South Korea.

Ommani, B., Kristiansen, T., Berget, K., Sandvik, P., Faltinsen, O., 2016. An investigation on moonpool blockage by box-shaped object close to free surface. Violent Flows 2016, Osaka, Japan.

Ommani, B., Kristiansen, T., Faltinsen, O.M., 2016. Simplified CFD modeling for bilge keel force and hull pressure distribution on a rotating cylinder. Appl. Ocean Res. 58, 253–265. https://doi.org/10.1016/j.apor.2016.04.010.

Ravinthrakumar, S., Kristiansen, T., Molin, B., Ommani, B., 2020. Coupled vessel and moonpool responses in regular and irregular waves. Appl. Ocean Res. 96, 102010. https://doi.org/10.1016/j.apor.2019.102010.

Rognebakke, O.F., Faltinsen, O.M., 2003. Coupling of sloshing and ship motions. J. Ship Res. 47 (3), 208–221.